Numerical simulation of strong blast waves in high temperature turbulent flows

S. Ghosh and K. Mahesh

Department of Aerospace Engineering and Mechanics
University of Minnesota, Minneapolis, MN, 55455, USA

Abstract

Numerical issues associated with simulating strong blast waves in high temperature flows in a turbulent background have been addressed effectively. Spherical energy deposition in both laminar and turbulent flows is considered. A predictor–corrector based shock capturing scheme is implemented along with a base spectral discretization scheme to simulate strong blast waves generated in the flow. The shock capturing scheme is extended for high temperature flows in equilibrium. Formulation of high temperature eigen vector matrices for 3–D Euler equations is presented for a generalized coordinate system. A logarithm formulation of the continuity equation is used to address stability issues related to very low densities in the core. A non-linear limiter has been implemented to eliminate excessive dissipation of the background turbulence due to shock capturing.

Introduction

There are important practical problems that involve very high temperature blast waves propagating through a turbulent medium. Examples of such problems are laser energy deposition in a turbulent background and discharge spark formation in a turbulent background. Propagation of strong blast waves in laminar flows has been studied theoretically [15, 13], experimentally [5, 10] and computationally [14, 7]. These problems involve stellar explosions [9], chemical explosions [1], laser energy deposition [5, 3] and energy deposition by a discharge spark [12].

The objective of this paper is to describe some of the numerical issues involved with accurate simulation of high temperature blast waves in a turbulent background. Specifically our interest is to simulate laser energy deposition in turbulent flows. Here, laser energy is deposited in a small volume of a gas. This results in formation and propagation of a blast wave through the background turbulence. Depending on the initial density of deposited laser energy, the initial temperatures could be as high as $50,000K$ and the blast wave generated can initially have Mach numbers as high as 8.0. Also, energy deposition results in sharp expansion of the core. Hence, densities in the core could be very low. Typically the minimum densities in the core could be 2 to 3 orders of magnitude smaller than the density of the surrounding fluid.

The Navier–Stokes equations with suitable modifications can be used as the governing equations. Presence of high temperatures lead to a number of reactions occurring in the flow e.g ionization, dissociation, recombination, charge exchange and charge transfer. Most recent simulations [8, 3] use a detailed chemistry model to simulate the conditions of chemical non–equilibrium existing in the flow. However these simulations are computationally very intensive. Hence only two dimensional simulations have been performed. A simpler equilibrium based model has been used for the simulations in this paper. The model does not use additional source terms in the Navier–Stokes equations. However the effect of all the above chemical reactions are taken into account by using equilibrium data for the thermodynamic quantities to obtain a closure for the system of governing equations. Thus the simulations are less expensive computationally and three dimensional simulation is possible even at the resolution required to simulate these high temperature flows. The three dimensional simulation is especially necessary for simulation of turbulence in the background.

Simulating such flows involve three primary numerical challenges: (i) accurate simulation of strong blast waves, (ii) stabilization of the solution in regions of low densities in the core and (iii) simulation of strong blast waves without excessive dissipation of the background turbulence. These issues are addressed in the following sections.

A parallel Fourier spectral solver with shock capturing capability has been developed. Given the fact that the boundary conditions are periodic, to allow the blast waves to propagate to very large distances the spectral method was developed for a domain whose size is adaptively increased in time. This is done by interpolating the solution from a smaller to a larger domain using a spectral interpolation scheme and is essential to study the long time evolution of the core.

Simulation methodology

The governing equations are the continuity, and compressible Navier–Stokes equations applied to a real gas,

$$\frac{\partial \rho}{\partial t} + \frac{\partial \rho u_i}{\partial x_i} = 0, \tag{1}$$

$$\frac{\partial \rho u_j}{\partial t} + \frac{\partial \rho u_j u_i}{\partial x_i} =$$
$$-\frac{\partial}{\partial x_i}\left[p\delta_{ij} - \frac{\mu(T)}{Re}\left(\frac{\partial u_i}{\partial x_j} + \frac{\partial u_j}{\partial x_i} - \frac{2}{3}\frac{\partial u_k}{\partial x_k}\delta_{ij}\right)\right], \tag{2}$$

$$\frac{\partial \rho e_T}{\partial t} + \frac{\partial \rho e_T u_i}{\partial x_i} =$$
$$\frac{\partial}{\partial x_i}\left[-pu_i + \frac{\mu(T)}{Re}\left(\frac{\partial u_i}{\partial x_j} + \frac{\partial u_j}{\partial x_i} - \frac{2}{3}\frac{\partial u_k}{\partial x_k}\delta_{ij}\right)u_j\right]$$
$$+ \frac{\partial}{\partial x_i}\left(\frac{\kappa(T)}{(\gamma-1)RePr}\frac{\partial T}{\partial x_i}\right) \tag{3}$$

where all the variables are non–dimensionalized with respect to their initial background values.

$$x_i = x_i{}^*/L_0{}^*,\ u_i = u_i{}^*/c_0{}^*,\ t = t^* c_0{}^*/L_0{}^*,$$
$$\rho = \rho^*/\rho_0{}^*,\ p = p^*/\rho_0{}^* c_0{}^{*2},\ T = T^*/T_0{}^*$$
$$\mu(T) = \mu(T)^*/\mu_0{}^*,\ \kappa(T) = \kappa(T)^*/\kappa_0{}^*. \tag{4}$$

Here, the subscript '0' denotes initial background values and the superscript, '*' denotes dimensional variables. L_0^* is the length scale and is obtained by comparing the non–dimensional size of the energy spot used in the simulations to its actual dimensional size. c_0^* is the speed of sound based on initial background temperature; i.e.
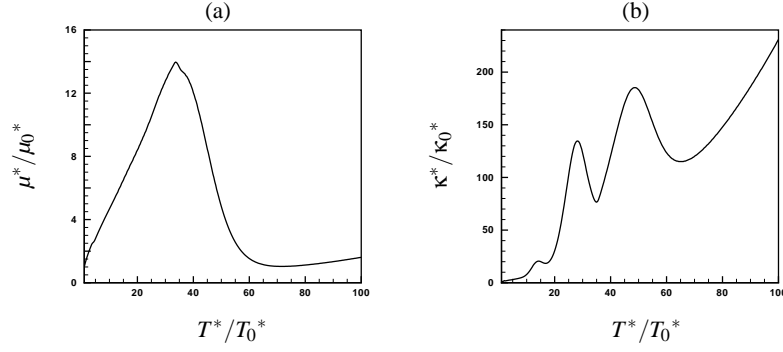
Figure 1: (a) Variation of the coefficient of viscosity μ with temperature T. (b) Variation of the coefficient of thermal conductivity κ with temperature T.

$$c_0^* = (\gamma_0 R_0^* T_0^*)^{1/2}. \tag{5}$$

$\mu(T)^*$ and $\kappa(T)^*$ are dimensional coefficients of viscosity and thermal conductivity obtained by assuming an equilibrium model for air (figure 1).

The equation of state is

$$p = \rho R(T) T, \tag{6}$$

where

$$R(T) = R^*(T)/\gamma_0 R_0, \tag{7}$$

and the variation of R^* with temperature is shown in figure 2b. The total energy is related to internal energy and kinetic energy as

$$\rho e_T = \rho e + \frac{1}{2}\rho u_i u_i. \tag{8}$$

and temperature is obtained from internal energy using the equilibrium dependence of internal energy on temperature shown in figure 2a.

The Reynolds number and Prandtl number are given by

$$Re = \rho_0^* c_0^* L_0^*/\mu_0^*, \quad Pr = \mu_0^* c_{p0}^*/\kappa_0^*. \tag{9}$$

c_{p0}^* is the specific heat at constant pressure at $T^* = T_0^*$.

The Navier–Stokes equations are solved using Fourier methods to compute the spatial derivatives. A collocated approach is used, and the solution is advanced in time using a fourth order Runge–Kutta scheme. The skew–symmetric form of the convection terms is used to suppress aliasing errors resulting from the nonlinear convection terms [2].

Numerical challenges

Shock capturing

Recall that a strong shock wave propagates through the flow domain, when energy is added instantaneously. Experiments in laser induced breakdown [16] show that the maximum temperature in the core is very high. This leads to sharp gradients in

the flow variables. Since the flow solver uses spectral methods for spatial discretization, resolving these sharp gradients requires a highly refined mesh. The computational cost therefore increases significantly with increasing core temperatures. The Fourier spectral method is therefore combined with a shock capturing scheme proposed by [17], to avoid resolution of the shock thickness.

The shock capturing scheme is based on the finite volume methodology, and is applied as a corrector step to the Fourier discretization used in this paper. In the first step, the predicted form of the solution vector is obtained using Fourier methods as discussed in the previous section. This solution vector is then corrected using the filter numerical fluxes obtained by using a characteristic based filter

$$U^{n+1} = \widehat{U}^{n+1} + \Delta t \left[\frac{1}{\Delta x}\left(\widetilde{F}^\star_{i+1/2,j,k} - \right.\right.$$
$$\left. \widetilde{F}^\star_{i-1/2,j,k} \right) + \frac{1}{\Delta y}\left(\widetilde{G}^\star_{i,j+1/2,k} - \widetilde{G}^\star_{i,j-1/2,k} \right)$$
$$\left. + \frac{1}{\Delta z}\left(\widetilde{H}^\star_{i,j,k+1/2} - \widetilde{H}^\star_{i,j,k-1/2} \right) \right] \tag{10}$$

The filter numerical flux vector is of the form

$$\widetilde{F}^\star_{i+1/2,j,k} = \frac{1}{2}R_{i+1/2,j,k}\phi^\star_{i+1/2,j,k} \tag{11}$$

where R is the right eigen vector matrix. The elements of $\phi^\star$ are denoted by $\phi^{l\star}$ and are given by

$$\phi^{l\star}_{i+1/2,j,k} = \kappa\theta^l_{i+1/2,j,k}\phi^l_{i+1/2,j,k} \tag{12}$$

The parameter κ is problem dependent and lies between 0.03 and 2 [17]. $\kappa = 1.0$ has been used in the simulations. The function $\theta^l_{i+1/2,j,k}$ is the Harten switch [6] and depends on the Left eigen vector matrix L. The formulation used for $\phi^l_{i+1/2,j,k}$ is given by the Harten–Yee upwind TVD form [17].

However for high temperature flows, the eigen vector matrices R and L need to be computed appropriately. The specific heats at constant pressure and volume C_P and C_V are no longer constants but depend strongly on temperature. Also, the internal
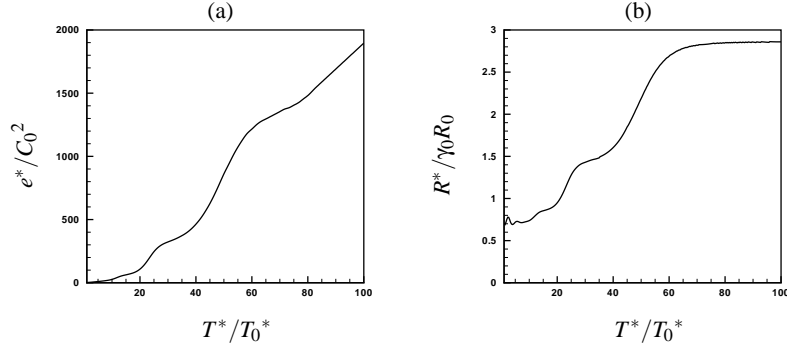
Figure 2: (a) Variation of internal energy e with temperature T, (b) Variation of R with temperature T.

energy and enthalpy can no longer be obtained from the simple relations

$$e = C_V T \quad ; \quad h = C_P T \qquad (13)$$

The sound speed is no longer obtained by

$$c = (\gamma R T)^{1/2} \qquad (14)$$

and R no longer remains constant, but becomes a function of temperature (figure 2b). Thus, to compute the eigen vector matrices, the Jacobian matrix $\frac{\partial \mathbf{F}}{\partial \mathbf{U}}$ needs to be recomputed. Here $\mathbf{F}$ denotes the flux vector

$$\bar{\mathbf{F}} = \begin{pmatrix} \rho v_n \\ \rho u v_n + p n_x \\ \rho v v_n + p n_y \\ \rho w v_n + p n_z \\ \rho h_0 v_n \end{pmatrix}$$

and $\mathbf{U}$ denotes the vector of the conserved variables

$$\bar{\mathbf{U}} = \begin{pmatrix} \rho \\ \rho u \\ \rho v \\ \rho w \\ \rho e_0 \end{pmatrix}.$$

$$v_n = u n_x + v n_y + w n_z \qquad (15)$$

and

$$n_x{}^2 + n_y{}^2 + n_z{}^2 = 1. \qquad (16)$$

h_0 is the total enthalpy given by

$$h_0 = h + e_k, \qquad (17)$$

where h is enthalpy and is given by

$$h = e + p/\rho. \qquad (18)$$

The equation of state for the gas is given by

$$p = \rho R(T) T. \qquad (19)$$

Then the elemental change in pressure dp can be written as

$$dp = RT d\rho + \rho \left(R + T \frac{dR}{dT} \right) dT. \qquad (20)$$

Now since $e = e(T)$,

$$dT = \left(\frac{dT}{de} \right) de \qquad (21)$$

where the internal energy e can be written in terms of the conservative variables u_i. Using the above relations the generalized Jacobian matrix can be computed as

$$\mathbf{J} = \begin{pmatrix} 0 & 1 \\ -u v_n + (RT - A(e - e_k))n_x & u n_x + v_n - A u n_x \\ -v v_n + (RT - A(e - e_k))n_y & v n_x - A u n_y \\ -w v_n + (RT - A(e - e_k))n_z & w n_x - A u n_z \\ -e_0 v_n - A v_n (e - e_k) & e_0 n_x + RT n_x - v_n A u \end{pmatrix}$$

$$\begin{pmatrix} 0 & 0 & 0 \\ u n_y - A v n_x & u n_z - A w n_x & A n_x \\ v n_y + v_n - A v n_y & v n_z - A w n_y & A n_y \\ w n_y - A v n_z & w n_z + v_n - A w n_z & A n_z \\ e_0 n_y + RT n_y - v_n A v & e_0 n_z + RT n_z - v_n A w & v_n (1 + A) \end{pmatrix}$$

where

$$e_0 = e + e_k \qquad (22)$$

is the total energy and e_k is the kinetic energy given by

$$e_k = \frac{1}{2} u_i u_i. \qquad (23)$$

The factor A is given by

$$A = \left(R + T \frac{dR}{dT} \right) \frac{dT}{de}. \qquad (24)$$

Note that evaluation of these Jacobian matrices requires the variation of e and R with temperature. This can be obtained for air assuming it to be composed of several species present under conditions of chemical and thermal equilibrium (figure 2).

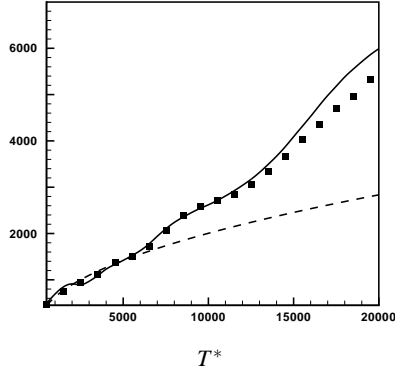The generalized eigen values of the above matrix are obtained as :

310

Figure 3: (a) Comparison of c_1 with data for speed of sound, ——— : speed of sound obtained from data, ▪ : computed speed of sound c_1, - - - - : $c = (\gamma_0 R_0 T)^{1/2}$

$$\lambda = \begin{pmatrix} v_n - c_1, & v_n, & v_n + c_1, & v_n, & v_n \end{pmatrix}$$

where the modified speed of sound c_1 is given by

$$c_1 = ((1+A)RT)^{1/2}. \tag{25}$$

Note that c_1 reduces to c for low temperatures and the Jacobian matrix reduces to the low temperature Jacobian. The modified sound speed depends on the variation of e and R with T through the factor A. c_1 has been computed and compared to data for speed of sound obtained assuming air as a mixture of multiple species in equilibrium (figure 3). Reasonable comparison is obtained up to $T^* = 15000K$.

The right eigen vector matrix **R** can be obtained by solving the system of equations

$$[J]R_i = \lambda_i R_i \tag{26}$$

where λ_i are the individual eigen values and R_i are the eigen vectors. Define a set of variables e_1 and e_2 such that

$$e_1 = \frac{c_1{}^2}{A(A+1)} \tag{27}$$

and

$$e_2 = e - e_1. \tag{28}$$

Also define $e_k{}^*$ such that

$$e_k{}^* = e_k - e_2. \tag{29}$$

Using these new variables a possible set of the right eigen vector matrices are obtained as

$$\mathbf{R_1} = \begin{pmatrix} 1 & 1 & 1 & 0 & 0 \\ u-c_1 n_x & u & u+c_1 n_x & n_y & -n_z \\ v-c_1 n_y & v & v+c_1 n_y & -n_x & 0 \\ w-c_1 n_z & w & w+c_1 n_z & 0 & n_x \\ h_0 - c_1 v_n & e_k{}^* & h_0 + c_1 v_n & un_y - vn_x & wn_x - un_z \end{pmatrix},$$

$$\mathbf{R_2} = \begin{pmatrix} 1 & 1 & 1 & 0 & 0 \\ u-c_1 n_x & u & u+c_1 n_x & n_y & 0 \\ v-c_1 n_y & v & v+c_1 n_y & -n_x & n_z \\ w-c_1 n_z & w & w+c_1 n_z & 0 & -n_y \\ h_0 - c_1 v_n & e_k{}^* & h_0 + c_1 v_n & un_y - vn_x & vn_z - wn_y \end{pmatrix},$$

$$\mathbf{R_3} = \begin{pmatrix} 1 & 1 & 1 & 0 & 0 \\ u-c_1 n_x & u & u+c_1 n_x & -n_z & 0 \\ v-c_1 n_y & v & v+c_1 n_y & 0 & n_z \\ w-c_1 n_z & w & w+c_1 n_z & n_x & -n_y \\ h_0 - c_1 v_n & e_k{}^* & h_0 + c_1 v_n & wn_x - un_z & vn_z - wn_y \end{pmatrix}.$$

Then the corresponding set of left eigen vector matrices can be obtained as

$$[L] = [R]^{-1}, \tag{30}$$

and they are given by

$$\mathbf{L_1} = \begin{pmatrix} \frac{Ae_k{}^*+c_1 v_n}{2c_1{}^2} & -\frac{Au+c_1 n_x}{2c_1{}^2} & -\frac{Av+c_1 n_y}{2c_1{}^2} & -\frac{Aw+c_1 n_z}{2c_1{}^2} & \frac{A}{2c_1{}^2} \\ \frac{c_1{}^2-Ae_k{}^*}{c_1{}^2} & \frac{Au}{c_1{}^2} & \frac{Av}{c_1{}^2} & \frac{Aw}{c_1{}^2} & -\frac{A}{c_1{}^2} \\ \frac{Ae_k{}^*-c_1 v_n}{2c_1{}^2} & -\frac{Au-c_1 n_x}{2c_1{}^2} & -\frac{Av-c_1 n_y}{2c_1{}^2} & -\frac{Aw-c_1 n_z}{2c_1{}^2} & \frac{A}{2c_1{}^2} \\ \frac{v-v_n n_y}{n_x} & n_y & \frac{n_y{}^2-1}{n_x} & \frac{n_y n_z}{n_x} & 0 \\ \frac{v_n n_z-w}{n_x} & -n_z & \frac{-n_y n_z}{n_x} & \frac{1-n_z{}^2}{n_x} & 0 \end{pmatrix},$$

$$\mathbf{L_2} = \begin{pmatrix} \frac{Ae_k{}^*+c_1 v_n}{2c_1{}^2} & -\frac{Au+c_1 n_x}{2c_1{}^2} & -\frac{Av+c_1 n_y}{2c_1{}^2} & -\frac{Aw+c_1 n_z}{2c_1{}^2} & \frac{A}{2c_1{}^2} \\ \frac{c_1{}^2-Ae_k{}^*}{c_1{}^2} & \frac{Au}{c_1{}^2} & \frac{Av}{c_1{}^2} & \frac{Aw}{c_1{}^2} & -\frac{A}{c_1{}^2} \\ \frac{Ae_k{}^*-c_1 v_n}{2c_1{}^2} & -\frac{Au-c_1 n_x}{2c_1{}^2} & -\frac{Av-c_1 n_y}{2c_1{}^2} & -\frac{Aw-c_1 n_z}{2c_1{}^2} & \frac{A}{2c_1{}^2} \\ \frac{v_n n_x-u}{n_y} & \frac{1-n_x{}^2}{n_y} & -n_x & \frac{-n_x n_z}{n_y} & 0 \\ \frac{w-v_n n_z}{n_y} & \frac{n_x n_z}{n_y} & n_z & \frac{n_z{}^2-1}{n_y} & 0 \end{pmatrix},$$

$$\mathbf{L_3} = \begin{pmatrix} \frac{Ae_k{}^*+c_1 v_n}{2c_1{}^2} & -\frac{Au+c_1 n_x}{2c_1{}^2} & -\frac{Av+c_1 n_y}{2c_1{}^2} & -\frac{Aw+c_1 n_z}{2c_1{}^2} & \frac{A}{2c_1{}^2} \\ \frac{c_1{}^2-Ae_k{}^*}{c_1{}^2} & \frac{Au}{c_1{}^2} & \frac{Av}{c_1{}^2} & \frac{Aw}{c_1{}^2} & -\frac{A}{c_1{}^2} \\ \frac{Ae_k{}^*-c_1 v_n}{2c_1{}^2} & -\frac{Au-c_1 n_x}{2c_1{}^2} & -\frac{Av-c_1 n_y}{2c_1{}^2} & -\frac{Aw-c_1 n_z}{2c_1{}^2} & \frac{A}{2c_1{}^2} \\ \frac{u-v_n n_x}{n_z} & \frac{n_x{}^2-1}{n_z} & \frac{n_x n_y}{n_z} & n_x & 0 \\ \frac{v_n n_y-v}{n_z} & \frac{-n_x n_y}{n_z} & \frac{1-n_y{}^2}{n_z} & -n_y & 0 \end{pmatrix}.$$

The right and left eigen vector matrix pairs along the x,y and z directions for a Cartesian coordinate system can be obtained from the above formulation by using suitable values of v_n, n_x, n_y and n_z.
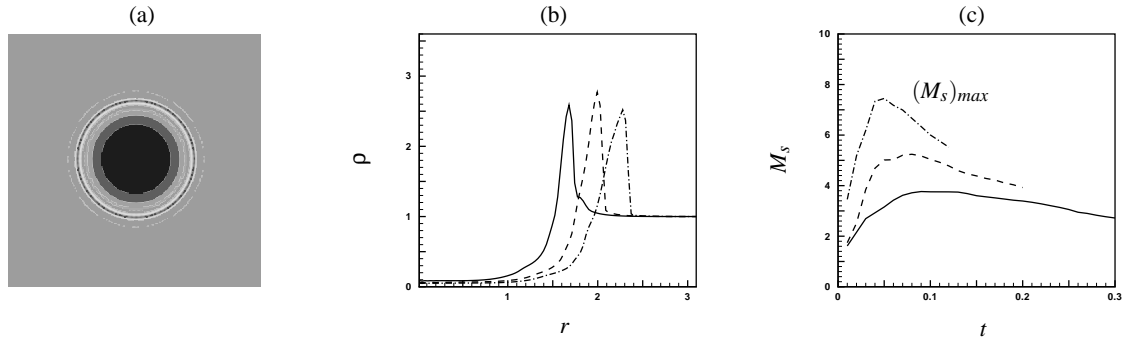
Figure 4: (a) Contours of pressure at $t = 0.2$ showing propagation of blast wave in flow at rest, (b) Radial profiles of the density at three different instants of time showing formation and propagation of a spherical blast wave, (c) Variation of shock Mach number with time ——— : $\Delta T_0 = 30$, ---- : $\Delta T_0 = 45$, —·—· : $\Delta T_0 = 60$.
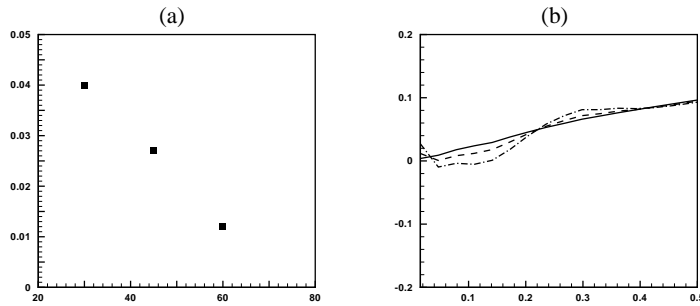

Figure 5: (a) Minimum values of density in the core for $\Delta T_0 = 30, 45$ and 60, (b) Radial profiles of density in the core at three successive time instants for $\Delta T_0 = 30$ showing that the simulation becomes unstable without the logarithmic formulation of the continuity equation.

Logarithm formulation of the continuity equation

When laser energy is added to a flow at rest, there is noticeable expansion at the core. This results in very small values of density at the core. When the continuity equation was advanced in time with density as the dependent variable, the solution was found to become unstable. It was therefore decided to solve for the logarithm of density as the variable. Define

$$v = \log \rho \qquad \Rightarrow \qquad \rho = e^v. \qquad (31)$$

The continuity equation becomes

$$\frac{\partial v}{\partial t} + u_i \frac{\partial v}{\partial x_i} = -\frac{\partial u_i}{\partial x_i}. \qquad (32)$$

Note that ρ is always positive when computed as e^v, even for very small values of ρ. The $\log \rho$ formulation of the continuity equation therefore makes the solution stable in regions of very low density.

Logarithm formulation of the continuity equation leads to non–conservative formulation of the Navier–Stokes equations. However the predictor–corrector based formulation of the shock capturing scheme used allows us to implement shock capturing even for the non–conservative system of equations.

Results

Spherical energy deposition

A spherical region of the flow is heated at the center of the domain by increasing the temperature and pressure instanta-neously at constant density. The initial temperature distribution has a Gaussian profile:

$$\underbrace{T - 1}_{\Delta T} \;=\; \underbrace{(T_0 - 1)}_{\Delta T_0} e^{-r^2/r_0^2} \qquad (33)$$

where the temperatures are non-dimensionalized by the ambient temperature. ΔT is the local temperature excess over the ambient value, and ΔT_0 is the maximum temperature excess at the core. r is the radial distance from the center and r_0 is the cut–off radius for the Gaussian profile, chosen to be $\pi/4$ in a domain of 2π.

The initial energy deposited, ΔE can be related to ΔT_0 by integrating,

$$\Delta E = \int_0^\infty \rho_\infty e(\Delta T) 4\pi r^2 dr, \qquad (34)$$

where $e(\Delta T)$ is obtained from figure 2a.

Simulation results are obtained for $\Delta T_0 = 30, 45$ and 60. These temperatures correspond to non dimensional energies $\Delta E = 767, 1132$ and 1651 respectively deposited in the flow domain. Figure 4a shows contours of pressure at $t = 0.2$ for a maximum temperature excess of 30 in the core. A spherically symmetric shock front is seen to propagate, compressing the flow ahead of it, while the flow behind it expands. Since the problem is spherically symmetric, mean values of the flow variables are computed in a radially symmetric manner and plotted as a function of radial distance from the center.

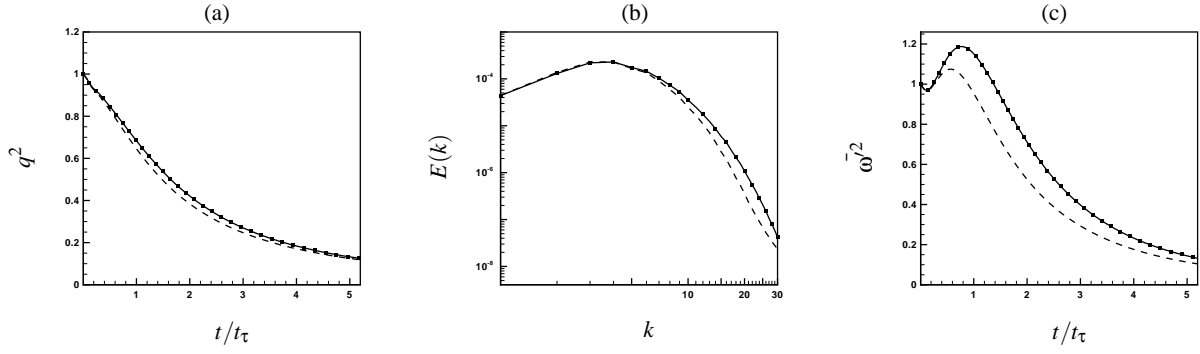Figure 4b shows radial profiles for density at three different in-

312

Figure 6: (a) Turbulent kinetic energy in time for isotropic turbulence, (b) Energy spectrum at $t/t_\tau = 5.0$, (c) Statistics for vorticity fluctuations, ——— without shock capturing, - - - - with shock capturing, ■ with shock capturing and nonlinear limiter.
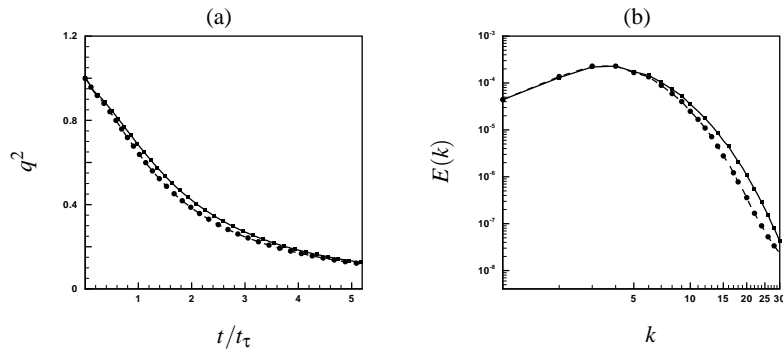

Figure 7: (a) Turbulent kinetic energy in time, (b) Energy spectrum at $t/t_\tau = 5.0$, ——— without $\log\rho$ formulation and without shock capturing, ■ with $\log\rho$ formulation and without shock capturing, - - - - without $\log\rho$ formulation and with shock capturing, ● with $\log\rho$ formulation and with shock capturing.

stants of time for $\Delta T_0 = 30$. Note that there is an initial period of time during which the intensity of the shock front increases with time, indicating formation of the shock. Once shock formation is complete, the shock wave propagates radially into the background gas, its strength decreasing as a result.

Figure 4c shows the variation of shock Mach number in time for $\Delta T_0 = 60, 45$ and 30. The shock Mach number can be computed using the relation

$$U_s = \frac{\gamma+1}{4}U + ((\frac{\gamma+1}{4}U)^2 + c_\infty^2)^{1/2}, \qquad (35)$$

for the shock velocity U_s. Here, U is the velocity behind the shock front and c_∞ is the speed of sound ahead of it. The initial steep increase in the shock Mach number depicts shock formation. The later gradual decrease in shock Mach number depicts the radial propagation of the shock. The shock Mach number attains a maximum value at the end of shock formation. The values of shock Mach number increase with increase in energy deposited. Note that the maximum shock Mach number varies from 3.77 to 7.45 for ΔT_0 changing from 30 to 60. Simulation of these strong blast waves is not possible without incorporation of the shock capturing scheme.

Figure 5a shows the minimum values of density in the core for $\Delta T_0 = 30, 45$ and 60. Note that the densities in the core are very low owing to rapid expansion during the shock formation process. Also the minimum value of density decreases with increase in ΔT_0. Figure 5b shows density in the core at three successive instants of time obtained from a solver that does not use the logarithm formulation of the continuity equation. The low

densities in the core result in the solution becoming unstable. Using the logarithm formulation, density is forced to be positive at all times and so a stable solution is obtained.

Isotropic turbulence

Direct numerical simulation of isotropic turbulence was performed under conditions corresponding to past DNS by Blaisdell et al. [2]. The initial velocity fluctuations are isotropic and divergence–free, while initial fluctuations in pressure, temperature and density are assumed to be zero. The initial velocity fluctuations are generated using Rogallo's method [11]. The Fourier coefficients of the initial velocity fields are given by

$$\hat{u} = \frac{\alpha k k_2 + \beta k_1 k_3}{k(k_1^2+k_2^2)^{1/2}}e_1 + \frac{\beta k_2 k_3 - \alpha k k_1}{k(k_1^2+k_2^2)^{1/2}}e_2 - \frac{\beta(k_1^2+k_2^2)^{1/2}}{k}e_3$$

$$(36)$$

where

$$\alpha(k) = \frac{E(k)}{4\pi k^2}^{1/2} e^{i\theta_1}\cos(\phi), \quad \beta(k) = \frac{E(k)}{4\pi k^2}^{1/2} e^{i\theta_2}\cos(\phi). \quad (37)$$

Here θ_1, θ_2 and ϕ are random numbers from 0 to 2π, and e_i denote the unit vectors along the three coordinate directions. The initial energy spectrum is $E(k) \sim k^4 e^{-k^2}$ and peaks at $k_0 = 5$. The initial fluctuation Mach number $M_t = 0.3$ and Taylor micro scale Reynolds number $Re_\lambda = 70$.

The effect of the shock capturing scheme on time evolution of this turbulent field is studied. Figure 6a shows time evolution of the turbulent kinetic energy. Note that the added dissipation from the shock capturing results in under–prediction of the turbulent kinetic energy. However, the shock capturing scheme is
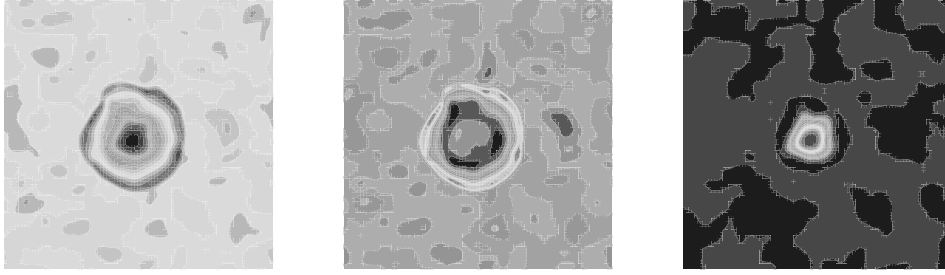
313

Figure 8: Contours of density, pressure and temperature at a given instant of time shows interaction of the spherical energy spot with a turbulent background.
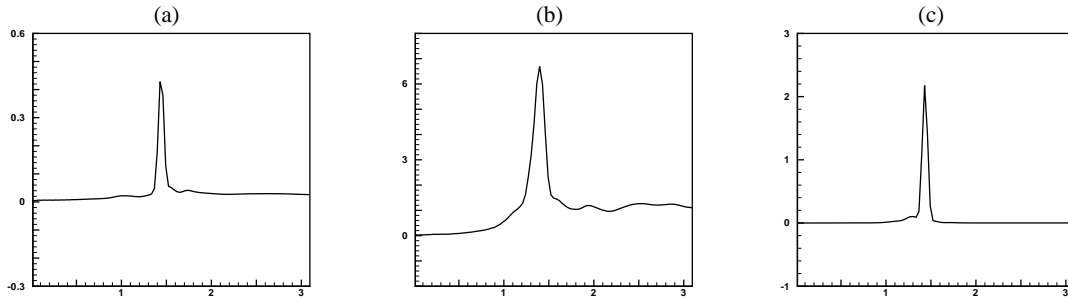

Figure 9: Radial statistics for (a) the radial component of velocity, (b) the transverse component of vorticity, and (c) pressure at $t = 0.19$ after energy deposition.

essential in the presence of strong shock waves. Thus, for accurate simulation of the the background turbulence a nonlinear limiter [4] has been implemented that turns on the shock capturing only in the vicinity of the shock wave. The limiter is given by

$$g = \frac{\theta^2}{\theta^2 + \omega^2}, \qquad (38)$$

where θ denotes divergence of velocity and ω denotes vorticity magnitude. Figure 6b shows the energy spectrum at $t/t_\tau = 5.0$ where t_τ denotes the eddy turn over time. Excessive dissipation due to shock capturing is evident. Note that use of the nonlinear limiter removes this excessive dissipation.

Figure 6c shows statistics for the time evolution of the vorticity fluctuations. Note that even for higher order quantities, the excessive dissipation introduced by the shock capturing scheme is effectively avoided using the nonlinear limiter.

The effect of using the logarithm formulation for the continuity equation on isotropic turbulence has been shown in figure 7. Figure 7a shows decay of turbulent kinetic energy in time while figure 7b shows energy spectrum computed at a given instant of time. Results are compared from two different solvers. The first one uses the normal formulation of the continuity equation while the second one uses the logarithm formulation. For each solver results are shown with and without the application of shock capturing. In both the cases, the logarithm formulation of the continuity equation is found to accurately compute the evolution of the turbulent field.

Spherical energy deposition in isotropic turbulence.

Consider spherical deposition of energy in background isotropic

turbulence. Energy is deposited as described in the section "Spherical energy deposition", while the turbulence is generated in the background as described in the section "Isotropic turbulence". The turbulent field is allowed to decay for some time after which the velocity derivative skew–ness attains a steady value in the range of -0.3 to -0.4. The energy spot is then introduced by increasing the temperature and pressure at constant density.

Figure 8 shows contours of density, pressure and temperature at a later instant of time. A spherically symmetric blast wave is observed to propagate through the background turbulence compressing the flow in a spherically symmetric manner. There is significant expansion in the core. As the blast wave propagates significantly into the background, it is observed to get distorted rapidly due to interaction with the turbulence.

Since the problem is radially symmetric, statistics were obtained as a function of radial distance from the center. Figure 9a shows statistics for the radial component of velocity at $t = 0.19$. Amplification of turbulence levels are observed in the vicinity of the blast wave. The local compression across the blast wave causes the turbulence levels to amplify. Also since the blast wave is radially symmetric the amplification is most pronounced in the radial component of the velocity and hence in the transverse component of the vorticity. This is observed in statistics for the transverse component of vorticity shown in figure 9b. Figure 9c shows statistics for pressure fluctuations and indicate amplification in the vicinity of the blast wave. Turbulence levels are observed to get suppressed in the core.

Conclusions

This paper addresses some of the numerical issues that are associated with simulation of strong blast waves in high temperature flows interacting with turbulent background. Direct nu-

314

merical simulation is used to simulate high temperature turbulent flows under equilibrium conditions. The base numerical scheme is spectral. A predictor corrector based shock capturing scheme is incorporated to capture strong blast waves that are observed in the flow. The shock capturing scheme has been extended for high temperature flows in equilibrium. Formulation of high temperature eigen vector matrices for 3–D Euler equations has been presented for a generalized coordinate system. Due to significant expansion, the densities in the core are observed to be very low. Slight oscillations can thus result in densities becoming negative and the solution becoming unstable. A logarithm formulation of the continuity equation has been used to address stability issues related to very low densities in the core. The shock capturing scheme was found to dissipate the background turbulence excessively. To avoid this, a non-linear limiter has been implemented that applies shock capturing only to the vicinity of the shock wave.

Three problems were considered to demonstrate the numerical issues. The first problem dealt with spherical energy deposition. The high temperature extension of the shock capturing scheme was found to be essential for stability of the simulation. Also a logarithm formulation of the continuity equation was required for the solution be stable in regions of low densities. The second problem dealt with simulation of isotropic turbulence. The shock capturing scheme caused excessive dissipation thus leading to under prediction of the turbulent kinetic energy and the turbulent energy spectrum. It was shown that this excessive dissipation could be avoided by using the above mentioned non–linear limiter. The third problem dealt with spherical energy deposition in background isotropic turbulence. It was shown that use of the shock capturing scheme along with the non–linear limiter and the logarithm formulation of the continuity equation was necessary to obtain a stable and accurate solution for both the blast wave and the background turbulence.

References

[1] Aravin, G. S., Vlasov, P. A., Karasevich, Yu. K., Makolkin, E. V. & Neigauz, N. G., Investigation of the mechanism of chemical ionization accompanying high-temperature oxidation of methane in shock waves, *Combustion, Explosion, and Shock Waves*, **18(1)**, 1982, 39–45.

[2] Blaisdell, G. A., Mansour, N. N., & Reynolds, W. C., Numerical simulations of compressible homogeneous turbulence, *Report No TF-50, Thermosciences Division, Department of Mechanical Engineering, Stanford University*, 1991.

[3] Dors, I.G. & Parigger, C.G., Computational fluid–dynamic model of laser induced breakdown in air, *Applied Optics*, **42(30)**, 2003.

[4] Ducros, F., Ferrand, V., Nicoud, F., Weber, C., Darracq, D., Gacherieu, C. & Poinsot, T., Large-eddy simulation of the shock/turbulence interaction, *J. Comput. Phys.*, **152**, 1999, 517–549.

[5] Glumac, N., Elliot, G. & Boguszko, M., Temporal and spatial evolution of the thermal structure of a laser spark in air, *AIAA paper*, 2005–0204.

[6] Harten, A., The artificial compression method for computation of shocks and contact discontinuities, *Math. Comp.*, **32**, 1978, 363.

[7] Jiang, Z., Takayama, K., Moosad, K. P. B., Onodera, O. & Sun, M., Numerical and experimental study of a micro-blast wave generated by pulsed laser beam focusing, *Shock waves*, **8**, 1998, 337–349.

[8] Kandala, R., & Candler, G., Numerical studies of laser–induced energy deposition for supersonic flow control, *AIAA paper*, 2003–1052.

[9] Kopal, G. & Lin, C. C., Propagation of spherical shock waves in stellar interiors, *Proceedings of the national academy of sciences*, **37 (8)**, 1951, 495–506.

[10] Phuoc, T. X., Laser spark ignition: Experimental determination of laser– induced breakdown thresholds of combustion gases, *Optics Communications*, **175(4)**, 2000, 419–423.

[11] Rogallo, R. S., Numerical experiments in homogeneous turbulence, *NASA Tech. Memo.*, 81315, 1981

[12] Shneyder, M. N., Macheret, S. O., Zaidi, S. H., Girgis, I. G., Raizer, Yu. P., & Miles, R. B., Steady and unsteady supersonic flow control with energy addition, *AIAA paper*, 2003–3862.

[13] Sedov, L. I., *Similarity and dimensional methods in mechanics*, Academic, New York, 1958.

[14] Steiner, H., Gretler, W. & Hirschler, T., Numerical solution for spherical laser–driven shock waves, *Shock waves*, **8**, 1998, 337–349.

[15] Taylor, G. I., The formation of a blast wave by a very intense explosion: I. theoretical discussion, *Proc. Roy. Soc.*, **201**, 1950, 159–174.

[16] Yan, H., Adelgren, M., Bouszko, M., Elliott, G.& Knight, D., Laser energy deposition in quiescent air, *AIAA paper*, 2003–1051.

[17] Yee, H. C., Sandham, N. D., Djomehri, M.J., Low–dissipative high–order shock–capturing methods using characteristic-based filter, *J. Comput. Phys.*, **150**, 1999, 199–238.